Optimal operation strategies of multi-energy systems integrated with liquid air energy storage using Information Gap Decision Theory

Caixin Yan[a,b], Chunsheng Wang[a,b,*], Yukun Hu[c], Minghui Yang[a,b], Hao Xie[a,b]

[a] School of Automation, Central South University, Changsha, 410083, China
[b] Hunan Xiangjiang Artificial Intelligence Academy, Changsha 410036, China
[c] Department of Civil, Environment & Geomatic Engineering, University College London, London WC1E 6BT, UK

Abstract

In this paper, a framework of multi-energy system (MES) integrating with a liquid air energy storage (LAES) system was proposed. LAES, where liquid air works as an energy storage media, is a powerful and eco-friendly technology for storing renewable energy resources and reducing grid curtailment. Considering the characteristics of LAES (i.e. cold and heat circulation), the incorporation of LAES system into the Combined Cooling, Heating and Power system can achieve integrated use of energy and effectively save energy. Moreover, the prices of electricity will affect the overall cost of the MES. In other words, the decision-makers of the MES need to consider the uncertainty of electricity prices when making power dispatching decisions. To model the uncertainty of electricity prices, the information gap decision theory method was used to study power dispatching strategies of the MES. Three different strategies were proposed, including risk-neutral, risk-averse and risk-taker. In addition, demand response algorithms were used to study load transfer strategies. The results show that the demand responses of the three strategies are effective in terms of load transfer and cost saving. The total operation cost in the risk-neutral strategy with demand response can be 6.82% less than that without demand response; In the risk-taker strategy with demand response, the allowable grid electricity price is reduced by 25.24% when the opportunity cost drops by $8,000, and 23.32% without demand response. With additional robustness cost, the acceptable price change ratio using demand response is 21.91% in the risk-averse strategy, and 20.04% without demand response.

Keywords: Multi-energy systems (MES); Liquid air energy storage (LAES); Information gap decision theory (IGDT); Demand response; Uncertainties

1. Introduction

Fossil fuel power generation remains a major part of power generation, and global energy demand is expected to continue to grow at a rate of 1.2% until 2040 [1]. Growing demand poses

* Corresponding author. E-mail address: wangcsu@csu.edu.cn (C. Wang)

a huge challenge to power producers who rely on fossil fuel power generation because existing fossil fuel power plants have been causing environmental problems. To meet the growing demand for energy, it is imperative to increase the penetration of renewable energy. Multi-energy systems (MES) [2], whereby electricity, heat, cooling, fuels, and so on optimally interact with each other at various levels, are considered as an effective system integration. For flexible operation of MES, energy storage is one of the essential components. Although the battery storage is technically mature and widely use in MES, it still has heavy metal pollution. For example, due to inaccurate information about waste lithium-ion batteries by third-party operators, it may cause leakage of chemically hazardous substances (such as nickel pollution) during the recycling process, and even battery pack explosions and fires [3]. Therefore, MES needs environmentally friendly energy storage as an alternative to achieve sustainable development.

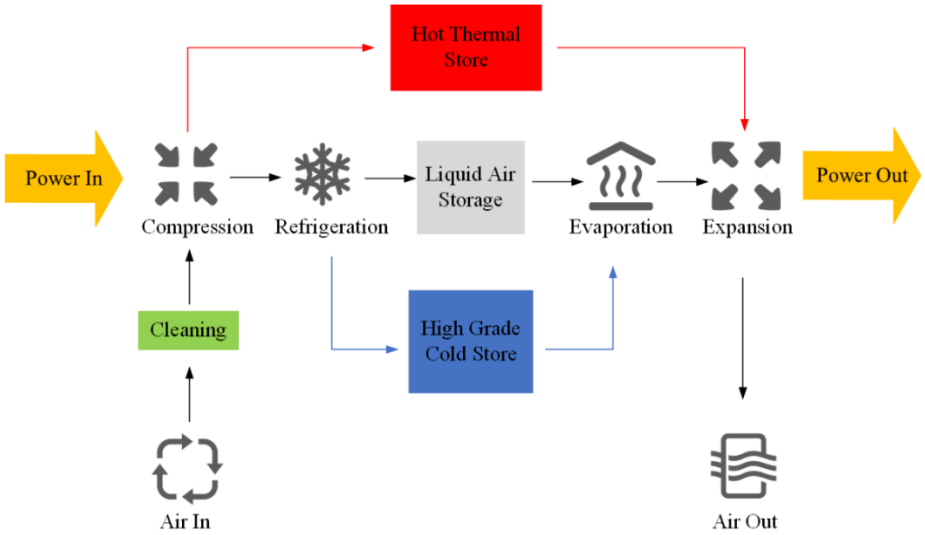

Figure 1. A process diagram of LAES

From an environmental perspective, mechanical energy storage is promising as it does not cause chemical pollution and therefore could be an alternative option [4]. There are two main types of mechanical energy storage [5]: Pumped Hydroelectric Energy Storage (PHES) and Compressed Air Energy Storage (CAES). The PHES is a mature technology of converting the mechanical energy of water in a storage dam into electrical energy [6]. However, the blockage and runoff changes caused by dam construction can cut off the spatial connectivity of the upstream and downstream, block the reproduction of upstream and downstream fish, flood a large amount of farmland and forest land, and finally destroy the original ecosystem. As for CAES, it is technology of converting the mechanical energy of compressed air in a large cave or tank into electrical energy. Although CAES does not need to change geography on a large scale, the limited available large caves and space-consuming tanks limit its application [7, 8]. An alternative technology of CAES is Liquid Air Energy Storage (LAES), where air is compressed into a denser liquid and therefore less space-consuming [9-11]. During the charging phase of LAES, the air from the environment is purified, compressed, refrigerated and eventually transferred to a cryogenic storage tank; and during the discharging phase of LAES (i.e. when the electric power generated by the MES is insufficient), the liquid air from the

cryogenic storage tank is pumped, evaporated, expanded and eventually generate electricity through the turbine. A complete charging-discharging phase of LAES within one day only losses 0.05% of the energy [12].

As shown in Figure 1, during the charging and discharging process of the LAES system, waste heat and cold energy will be generated as by-products and they can be either stored and reused in the system or can be accommodated by other systems. Many researchers have investigated effective ways of using these waste energies. For example, on the one hand, the waste thermal energy generated in the LAES system can be used as a heat source. Tafone et al. [13] solved the problem of insufficient waste heat utilization during LAES charging phase by integrating with Organic Rankine Cycle (ORC), thereby achieving the purpose of improving round-trip efficiency of the whole system. Ameel et al. [14] proposed a modified combined Rankine-liquefaction cycle through thermodynamic analysis to utilize the waste heat generated in the LAES system. Zhang et al. [15] investigated the system integration of using LAES waste heat for liquefied natural gas gasification. On the other hand, the waste cold energy generated in the LAES system can be used as a cold source. Rehman et al. [16] proposed a liquefied biomethane and LAES integrated system to use the waste cold energy to liquefy the biomethane, so as to reduce the load of refrigeration cycle. Li et al. [17] proposed a novel solution by integrating nuclear power generation with LAES to achieve an effective time shift of the electrical power output and provide an efficient way to use thermal energy of nuclear power plants in the LAES discharging process. Inspirited by these previous works, in this study we propose an integrated system of LAES and MES (i.e. LAES-MES), and the MES consists of a photovoltaic (PV) system, a wind power system, and a CCHP system. The LAES system could interact with the converter components of the CCHP system, such as combined heating and power, auxiliary boiler, absorption chiller and electric chiller, to realize the complementary utilization of power, thermal energy and cold energy.

Although many efforts have been made in system integration, only a few studies have focused on the economics of LAES integrated systems. The actual cost of the integrated system is affected by various elements, such as actual power generation, electricity price, transmission network reliability, equipment reliability, and actual load demand. For example, due to the uncertainty of solar radiation, the PV power generation is intermittent, fluctuant and unstable [18]. Inaccurate estimation of PV power generation will cause power curtailment and negatively affect revenue. These issues related to PV power generation may also exist in wind power generation [19, 20]. When these issues lead to system failure, the operation of the entire integrated system will be affected, and the maintenance of MES will be very costly [21].

Currently, there are many methods that can be used to deal with uncertainty issues and achieve optimal operation of integrated systems [22, 23]. Previous methods include deterministic [24], stochastic programming [25], robust optimization [26], interval optimization [27], Z-number [28], Fuzzy approach [29] and information gap decision theory [30]. The most widely used methods are stochastic programming and robust optimization. Vahid-Pakdel et al. [31] proposed a stochastic programming method to model the uncertainties (including demands, prices of the energy market and wind speed), in which Monte Carlo method was used to generate

corresponding deterministic probability distribution scenarios. Moazeni et al. [32] investigated a cost function approximation-based stochastic dynamic programming method to model the prices and demand uncertainties. Park et al. [33] proposed a two-stage stochastic programming method, in which distribution of load and wind power generation are generated by Gaussian copula method. Maghouli et al. [34] proposed a multi-stage and multi-objective stochastic programming method to model the uncertainty of generation capacity, in which Non-dominated Sorting Genetic Algorithm solved the computational difficulties. However, the optimal operation that based on stochastic programming depends on a specific probability distribution, which is restricted when information disclosure is insufficient. And stochastic programming is generally used in simple (linear) models. When applied in nonlinear models, it is computationally complex. In view of the problems in the above research, robust optimization methods that do not rely on detailed probability density functions are widely used. The basic idea of robust optimization is to realize investment decision or system operation under uncertainty. Among robust optimization methods, the most common methods are affinely adjustable robust optimization and adaptive robust optimization. For example, Moretti et al. proposed an affinely adjustable robust optimization method to obtain a scheduling solution for MES, taking into account uncertain loads and the generation of renewable energy [35]. Considering the uncertainty of load and energy prices, an adaptive robust optimization integrated bidding strategy was also proposed to enable the proposed MES to participate in day-ahead market [36]. However, these methods can only propose one strategy, which will cause the system managers to be unable to cope with the changing markets.

Compared with the above approaches, Information Gap Decision Theory (IGDT) method can meet the various needs of system operators in responding to the changing market, because it includes both opportunity function and robustness function [37]. The risk-taker and risk-averse strategy proposed can meet the requirements of system operation, and also maximize uncertainty tolerance under various budget requirements. IGDT method can also model the gap between the predicted and actual values of uncertain parameters without having to assume the probability distribution of uncertainty. This means that unlike other methods, the data of uncertainty is not highly demanded when IGDT method is applied to the model uncertainty. Therefore, when it is difficult to express uncertainty or the parameter data is seriously missing in the calculation of the system optimization operation, the system decision-makers can make an informed decision based on the IGDT.

Many researchers have studied the IGDT method to model the uncertainty of MES, so as to obtain investment schemes or operation strategies and achieve economic benefits. For example, Majidi et al. used the IGDT method to model the uncertainty of load demand to achieve optimal system operation [38]. Moghaddas-Tafreshi et al. used the IGDT to model the uncertainty of load demand for plug-in hybrid electric vehicles [39]. Also, Dolatabadi et al. proposed a hybrid method to minimize the operation costs of wind-based MES, and employed the IGDT to consider the uncertainty of electricity prices [40]. In addition to these, an IGDT-based energy scheduling strategy was proposed to take into account the uncertainty of renewable energy generation [41]. It can be seen that IGDT method is suitable to propose a corresponding and complete energy dispatching strategies for the uncertainty of a single variable.

If the electricity price of grid accessed is higher than expected, the purchase cost of LAES-MES will be higher than before, thereby increasing economic costs. Moreover, the uncertainty of the electricity prices means that the bidding strategy of LAES-MES to the operator of the grid accessed is unknown [42]. If the purchasing cost of LAES-MES is unknown, this will result in the inability to formulate an accurate capital budget, thereby reducing the efficiency of capital utilization. In addition, different electricity prices might affect supply schedules, and change the switching status of specific devices, thereby affecting the self-dispatching operation [43]. Therefore, it is necessary to formulate sufficient energy purchasing strategies for the changes in electricity prices on the operating cost of the LAES-MES system, which will help improve the stability of the system and the ability to resist risks.

In general, considering the characteristics of PV power generation, wind power generation, LAES, and CCHP, how to integrate them to make the best use of them, how to model the uncertainty of PV and wind power generation to minimize the impact on actual system operation, are pivotal problems need to solve. The novelty and contributions of this paper are summarized as follows:

(1) The development of a novel energy hub framework of LAES-MES, including combination of PV, wind power, LAES, and CCHP system;

(2) The theoretical analysis of coupling between CCHP system and LAES system;

(3) The demonstration of IGDT method applied on the LAES-MES system to optimize economy benefit by integrating diverse energy carriers;

(4) The assessment of three risk-based handling strategies based on IGDT method to address the challenge of uncertainty in electricity prices;

(5) The simulation analysis and results discussion to verify proposed control methods in LAES-MES system.

2. Scoping for simulation of the proposed LAES-MES

The proposed LAES-MES is shown in Figure 2, which includes electrical, heating, and cooling hubs to connect renewable energy systems (PV and wind power), natural gas system, CCHP system (including CHP, auxiliary boiler, absorption chiller and electric chiller), and LAES system. During operation, the thermal energy generated by the LAES compression is fed into the heating hub, while providing the LAES with thermal energy for liquid air expansion as needed. The cold energy generated by the LAES evaporation is fed into the cooling hub, while providing the LAES with cold energy for air refrigeration as needed. The LAES acts as electrical power storage. The pressure and temperature control units coordinate between the hub (i.e. PTCUH and PTCUC) and the storage sit to ensure the stable operation of the system. The objective function of the LAES-MES is to minimize the economic cost. Demand response program (DRP) was used to flat peak load and reduce energy purchasing cost in this study.

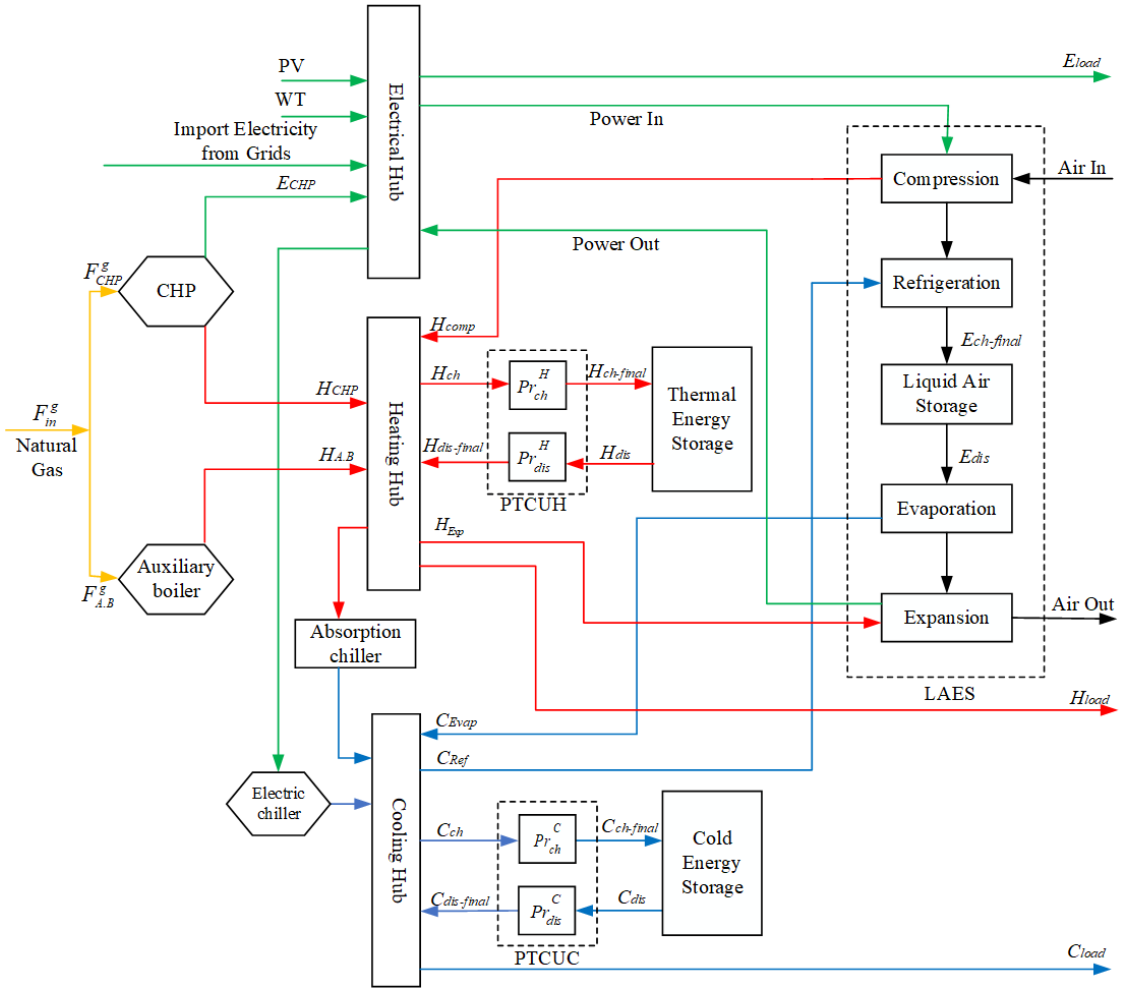

Figure 2. Frame of the LAES-MES

2.1 Objective function

The LAES-MES aims to minimize the economic cost considering constraints including energy prices, installed capacity and load demand. The objective function expression used is as follows:

$$\text{Min } \Gamma = \sum_{t=1}^{24} \left[Cost_g(t) + Cost_e(t) + Cost_m(t) \right] \tag{1}$$

The cost function for each component, including the natural gas ($Cost_g$), electrical power ($Cost_e$), maintenance cost ($Cost_m$), is given in Eqs. (2) - (4), respectively. They form the majority part of the economic cost of the system. It should be noted that this study studied the impact of uncertain electricity prices on the system economy and all the devices have been set without considering the installation and replacement cost.

$$Cost_g(t) = P^{g}_{CHP}(t) \times Pr_C(t) + P^{g}_{A.B}(t) \times Pr_A(t) \tag{2}$$

$$Cost_e(t) = E_{Grid}(t) \times Pr_e(t) \tag{3}$$

$$
\begin{aligned}
Cost_{es}(t) = {} & \xi_{oc}^{LAES} \times \left[E_{ch}(t) + E_{dis}(t)\right] + \xi_{oc}^{C} \times \left[C_{ch}(t) + C_{dis}(t)\right] + \xi_{oc}^{H} \times \left[H_{ch}(t) + H_{dis}(t)\right] \\
& + \xi^{PV} \times E_{PV}(t) + \xi^{WT} \times E_{WT}(t) + \xi^{A.B} \times H_{A.B}(t) + \xi^{Ab.chiller} \times C_{Ab.chiller}(t) \\
& + \xi^{EC} \times C_{EC}(t) + \xi^{CHP} \times E_{CHP}(t)
\end{aligned} \tag{4}
$$

2.2 Demand response modeling

The DRP is widely used to smooth load profiles and improve productivity [44]. In this study, time-of-use (TOU) rate [45] of DRP was used. The electricity prices at peak times are higher than that at off-peak times. According to TOU, partial load shifts from the peak times to the off-peak times will flat the load curve, and could reduce the installed capacity and the purchasing cost of LAES-MES. The function of TOU program was given in Eqs. (5) and (6).

$$
E_{load}(\mathrm{t}) = (1 - DR(t)) \times E_{load}^{b}(t) + E_{load}^{sh}(t) \tag{5}
$$

$$
E_{load}^{b}(t) - E_{load}(t) = DR(t) \times E_{load}^{b}(t) - E_{load}^{sh}(t) \tag{6}
$$

The corresponding constraints in the DRP are shown in Eqs. (7) - (10). Eq. (7) shows that the load which shifted from other times during total time periods should be equal to the load decreased during total time periods. That is to say, the total load remains constant before and after implementing DRP. The shifted load should not exceed a certain percentage of basic load in Eq. (8). Eqs. (9) and (10) express that the proportion of decrease and increase of load should not exceed a certain value, respectively. In this study, the maximum percentages are set to 20%.

$$
\sum_{t=1}^{24} E_{load}^{sh}(t) = \sum_{t=1}^{24} \left[DR(t) \times E_{load}^{b}(t) \right] \tag{7}
$$

$$
E_{load}^{sh}(t) \le inc(t) \times E_{load}^{b}(t) \tag{8}
$$

$$
DR(t) \le DR_{\max} \tag{9}
$$

$$
inc(t) \le inc_{\max} \tag{10}
$$

2.3 Constraints on subsystems

List capacity and application range of each subsystem device, which is helpful for LAES-MES manager to know the capacity of existing subsystems, and purchase devices reasonably and economically. And, each device is operating within its rated range, which can protect devices and prolong the service life of devices, so as to reduce maintenance costs and ensure the safety of the LAES-MES. The specific constraints of each subsystem (i.e. Constraints (A.1) - (A.45)) are listed in appendix A.

3. IGDT method

IGDT method is an effective interval optimization operation method considering the uncertainty of variables. Two opposite functions (i.e. robustness and opportunity function) are calculated to obtain the basis of decision when decision-makers are trapped in information

uncertainty. There are three components in the base model of IGDT, including (A) System model, (B) Uncertainty model and (C) Operation requirements.

3.1 System model

The system model of IGDT method is expressed as Eq. (11), and $F(P, \lambda)$ denotes the system model, $H(P, \lambda)=0$ and $G(P, \lambda) \geqslant 0$ represent equality constraints and inequality constraints of the system, respectively.

$$\begin{cases} \max\limits_{\lambda} \ F(P,\lambda) \\ s.t.\ H(P,\lambda)=0 \\ \quad\ G(P,\lambda) \geq 0 \end{cases} \tag{11}$$

where P and λ denote the decision variable and the uncertain parameter, respectively. According to the system model, a strategy can be studied before uncertainty is known, that is, system decision makers can regulate the system without risks of uncertainty. The strategy of the base case regards as risk-neutral strategy.

3.2 Uncertainty model

In IGDT, the uncertainty model represents the limit interval of uncertain parameter values. That is, it shows the maximum and minimum fluctuation range of the uncertain parameter. The mathematical expression is shown in Eq. (12).

$$\mathrm{U}(\alpha, \hat{\lambda}_t) = \left\{ \lambda_t : \frac{\left|\lambda_t - \hat{\lambda}_t\right|}{\hat{\lambda}_t} \leq \alpha \right\}, \alpha \geq 0 \tag{12}$$

where $\widehat{\lambda_t}$ and λ_t denote predicted and actual value of the uncertain parameter, respectively. And, α denotes the uncertain radius.

3.3 Operation requirements

IGDT is divided into a robust optimization model and an opportunity cost model, as shown in Eqs. (13) and (14), respectively. Under the condition that the decision result $F(P, \lambda)$ is not less than a certain robustness target F^a, the robustness function $\hat{\alpha}(F^a)$ is defined as the maximum fluctuation range of the allowable uncertain parameter λ, which is usually used by risk-averse decision-makers. On the contrary, under the condition that the decision result $F(P, \lambda)$ is higher than a certain opportunity target F^t, the opportunity function $\hat{\beta}(F^t)$ is defined as the minimum fluctuation range of the allowable uncertain parameter λ, which is usually used by risk-taker decision-makers.

$$\begin{aligned} \hat{\alpha}(F^a) &= \max\left\{\alpha : \text{minimum operation profit which is not less than a given profit target}\right\} \\ &= \max\left\{\alpha : \min(F(P,\lambda)) \geq F^a\right\} \end{aligned} \tag{13}$$

$$\begin{aligned} \tilde{\beta}(F^t) &= \min\left\{\beta : \text{maximum operation profit which is higher than a specified profit target}\right\} \\ &= \min\left\{\alpha : \max(F(P,\lambda)) \geq F^t\right\} \end{aligned} \tag{14}$$

After modelling uncertainty and fulfilling operational requirements, two strategies for dealing with uncertainty can be proposed in two functions (i.e. robustness and opportunity functions), which regard as risk-averse strategy and risk-taker strategy, respectively.

4. Three Strategies to deal with the uncertainty of electricity prices

According to the above discussion, solutions to solve the uncertainty of electricity prices that the IGDT method provides can be divided into three strategies [46]: A) Risk-neutral strategy; B) Risk-taker strategy; C) Risk-averse strategy.

4.1. Risk-neutral strategy

The risk-neutral strategy is the benchmark strategy of the IGDT method. The purpose is to get a predicted economic cost with predicted electricity prices. Its value is got under the hypothesis that there is no uncertainty. That is to say, the value of the robustness function and the opportunity function are both 0. The detailed mathematical expression is depicted as follows:

$$\text{Min } \Gamma=\sum_{t=1}^{24}\left[Cost'(t)+E_{Grid}(t)\times Pr_e(t)\right] \tag{15}$$

Subject to:

$$\text{Eqs. (1)-(10)} \tag{16}$$

$$\text{Constraints. (A.1)-(A.45)} \tag{17}$$

To make this easier to follow, total cost is divided into two parts which are depicted in Eq. (15), where $Cost'(t)$ denotes the cost without considering the amount of electricity purchased from the grid.

In practice, there is a striking difference between actual electricity prices and predicted electricity prices. So, risk-taker strategy and risk-averse strategy were introduced as follows due to the difference in actual electricity prices.

4.2. Risk-taker strategy

For the risk-taker decision-makers, the opportunity function $\hat{\beta}(R^t)$ represents the pursuit of smaller cost. To be specific, it means a power distribution strategy under low electricity selling cost. That is to say, the lower electricity price is, the smaller cost operators will spend. Therefore, opportunity function is shown by Eq. (18).

$$\hat{\beta}(R^t)=\text{Min}\left[\alpha:\left(\underset{Pr_e(t)\in U(\alpha,\tilde{Pr}_e(t))}{\text{Max}}\Gamma(E(t),Pr_e(t))\le R^t=(1+\delta)R^0\right)\right] \tag{18}$$

where R^t denotes the desired economic cost that the decision-makers hope to derive, or opportunity cost. And R^0 denotes the predicted economic cost which is calculated from Eqs. (1) - (10) and Constraints (A.1) - (A.45) based on the predicted electricity prices, δ denotes an opportunity cost deviation factor.

On the other hand, the smallest value α can be calculated in Eq. (19). Also, the maximum actual

electricity price is equal to $(1+\alpha)\widehat{Pr_e}(t)$. Therefore, the opportunity problem can be solved in Eqs. (19) - (23).

$$\hat{\beta}(R^t) = \min \alpha \tag{19}$$

Subject to:

$$\text{Min}\sum_{t=1}^{24}\left[Cost'(t)+E_{Grid}(t)\times Pr_e(t)\right] \le R^t = (1+\delta)R^0 \tag{20}$$

$$Pr_e(t)=(1+\alpha)\hat{P}r_e(t) \tag{21}$$

$$\text{Eqs. (1)-(10)} \tag{22}$$

$$\text{Constraints. (A.1)-(A.45)} \tag{23}$$

4.3. Risk-averse strategy

For the risk-averse decision-makers, the robustness function $\hat{\alpha}(R^a)$ represents the pursuit of stable cost. To be specific, it means a power distribution strategy that can stand up to the maximum fluctuations in electricity prices on the basis of realizing the expected cost. Therefore, the robustness function is shown by Eq. (24).

$$\hat{\alpha}(R^a)=\text{Max}\left[\alpha:\left(\underset{Pr_e(t)\in U(\alpha,\hat{P}r_e(t))}{\text{Min}}\Gamma(E(t),Pr_e(t)) \le R^a = (1-\chi)R^0\right)\right] \tag{24}$$

where R^a denotes the stable economic cost that the decision-makers hope to derive, or robustness cost. And χ denotes a robustness cost deviation factor.

On the other hand, the largest value α can be calculated in Eq. (25). Also, the minimum actual electricity price is equal to $(1-\alpha)\widehat{Pr_e}(t)$, respectively. Therefore, the robustness problem can be solved in Eqs. (25) - (29).

$$\hat{\alpha}(R^a) = \max \alpha \tag{25}$$

Subject to:

$$\text{Min}\sum_{t=1}^{24}\left[Cost'(t)+E_{Grid}(t)\times Pr_e(t)\right] \le R^a \tag{26}$$

$$Pr_e(t)=(1-\alpha)\hat{P}r_e(t) \tag{27}$$

$$\text{Eqs. (1)-(10)} \tag{28}$$

$$\text{Constraints. (A.1)-(A.45)} \tag{29}$$

5. Results and discussion

The main objective of the proposed strategies is to minimize the risk-constrained economic cost of the LAES-MES of a typical day by considering the uncertainty of electricity prices. To solve the economic operation problem of the LAES-MES that modeled as a mixed integer nonlinear program (MINLP), DICOPT solver under GAMS optimization software [47] was employed. In

Section 5.1, input data are showed, and the corresponding results of three strategies are presented in Section 5.2.

5.1. Input data

The electricity prices and natural gas prices forecast are shown in Figure 3, in which the electricity prices sold to the load is hypothesized to be equal to the electricity prices purchased from the grid in this study [3]. It should be noted that up to 20 percent of the base electrical load can be transferred, which means that $DR_{\max}$=20% and $inc_{\max}$=20%.

5.1.1 Load

In this study, loads (including electricity, thermal and cold load) are modeled using a Gaussian distribution [48].

$$PDF(E_{load}(t)) = \frac{1}{\sqrt{2\pi\sigma_{EL}^2}} e^{-\frac{(L-\mu_{EL})^2}{2\sigma_{EL}^2}} \tag{30}$$

$$PDF(H_{load}(t)) = \frac{1}{\sqrt{2\pi\sigma_{HL}^2}} e^{-\frac{(L-\mu_{HL})^2}{2\sigma_{HL}^2}} \tag{31}$$

$$PDF(C_{load}(t)) = \frac{1}{\sqrt{2\pi\sigma_{CL}^2}} e^{-\frac{(L-\mu_{CL})^2}{2\sigma_{CL}^2}} \tag{32}$$

where σ and μ denote the standard deviation and mean for load values, respectively.

5.1.2 Wind speed

Here, Weibull distribution is applied to model the wind speed [49].

$$PDF(\varpi) = (\frac{k}{c})(\frac{\varpi}{c})^{k-1} e^{(-\frac{\varpi}{c})^k} \tag{33}$$

where k is the shape parameter, and c is the scale parameter.

5.1.3 Solar irradiance

The solar irradiance is modeled using beta distribution [50]. The detailed equation is followed:

$$PDF(G(t)) = \begin{cases} \frac{\Gamma(\alpha+\beta)}{\Gamma(\alpha)+\Gamma(\beta)} \times G^{\alpha-1}(t) \times (1-G(t))^{\beta-1}, \ for\ 0 \le G(t) \le 1, \alpha, \beta \ge 0 \\ 0, \quad \text{else} \end{cases} \tag{34}$$

where α, β are the parameters of the beta distribution.

The results about wind power and PV generation system are presented in Figures 5 and 6, respectively.

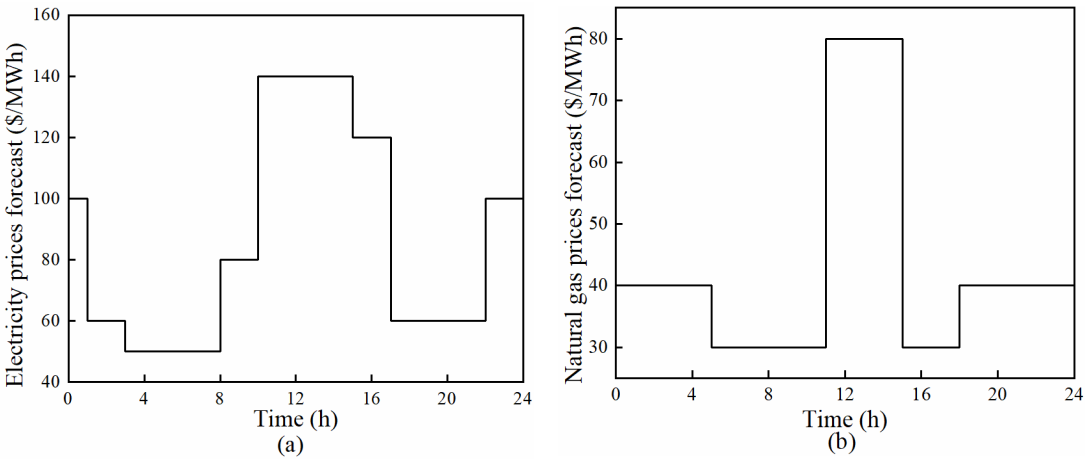

Figure 3. (a) Electricity prices and (b) Natural gas prices forecast

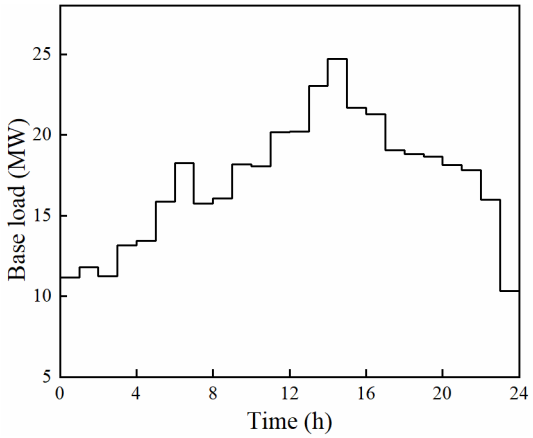

Figure 4. Base load demand

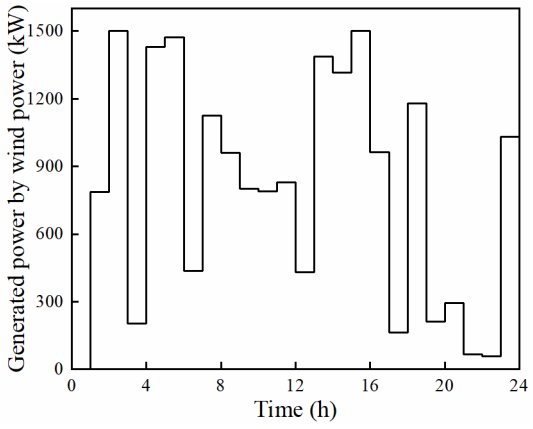

Figure 5. The generated power of wind power system

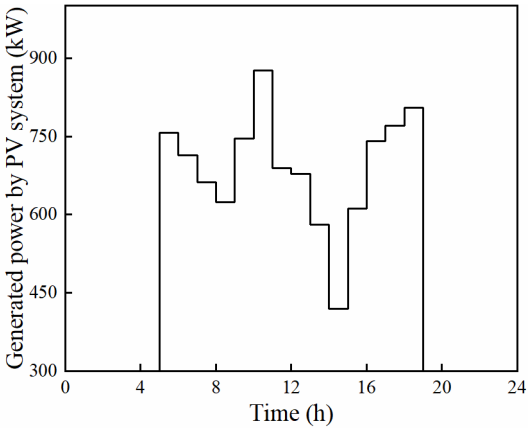

Figure 6. The generated power of PV system

5.2. Risk-neutral results

The risk-neutral results were obtained by assuming that actual electricity prices were equal to the predicted values. In the IGDT method, the risk-neutral strategy means that the value of robustness function and opportunity function is 0 (i.e. $\alpha = 0$ and $\beta = 0$). In this strategy, two cases were studied: without and with implementing DRP.

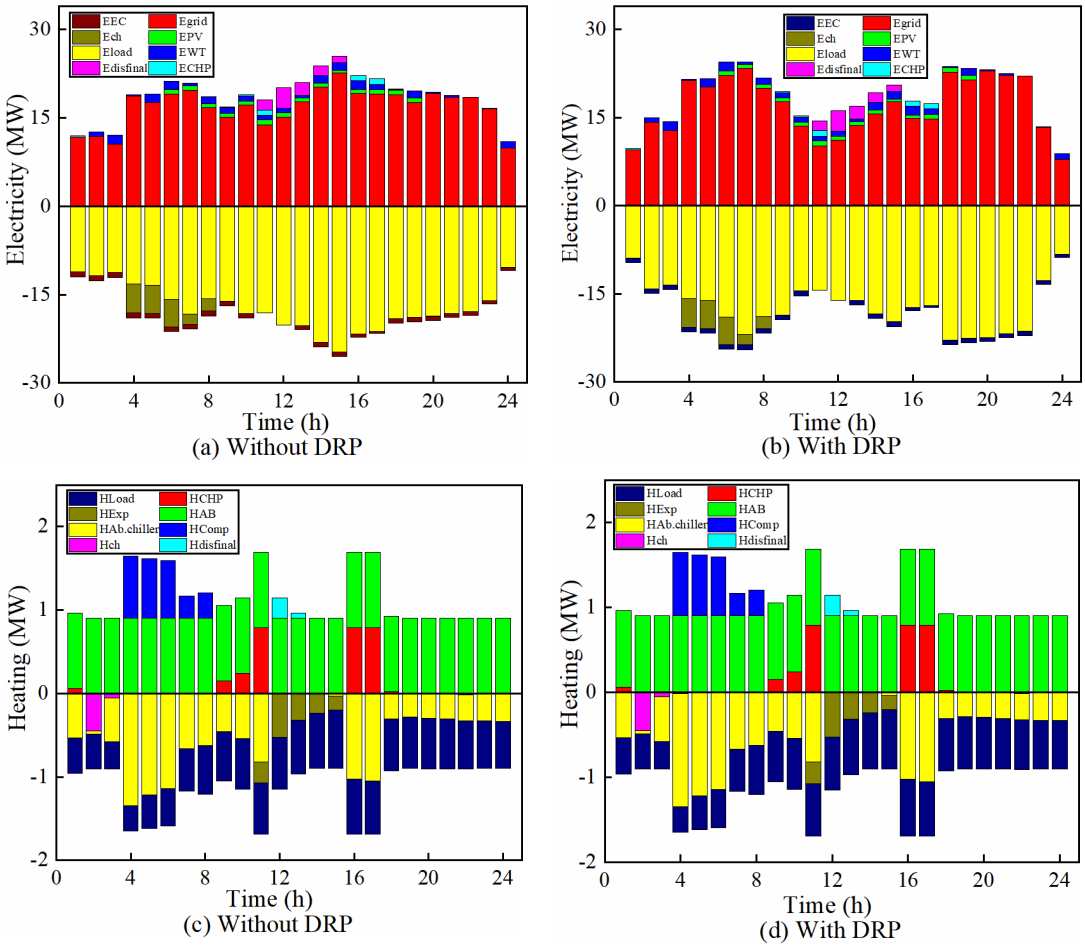

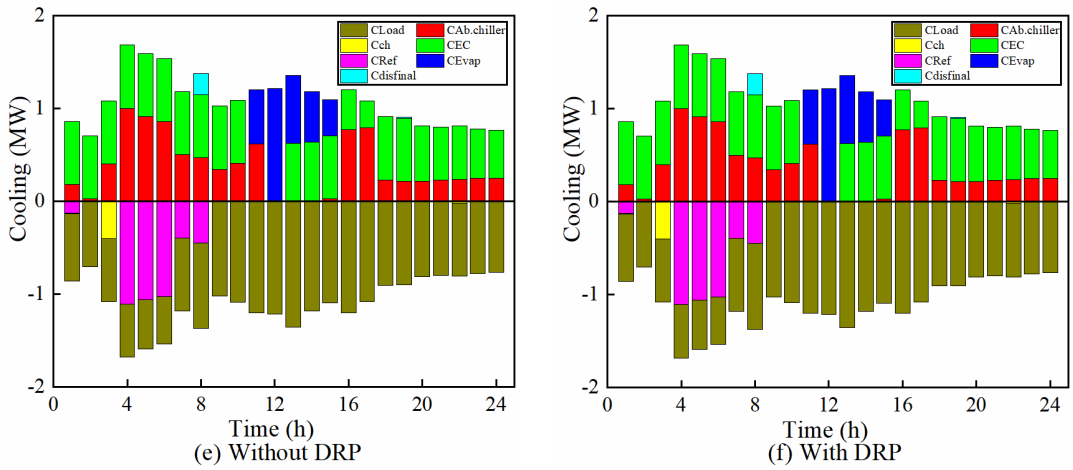

Figure 7. The operation strategies of three energy hubs

The operation statuses of three energy hubs are shown in Figure 7. The upper part of the horizontal axis y=0 line represents the total power flowing into the corresponding hub, and the lower represents the total power output by the corresponding hub. It can be seen that the total power in each time period is keeping balanced. The electrical hubs of the two cases are shown in Figure 7(a) and (b), respectively. The grid undertakes most of the electricity supply of the LAES-MES, and then renewable energy power generation (i.e. PV and wind power) undertakes some of the electricity supply. Natural gas (i.e. E_{CHP}) provides the least electricity supply. The LAES charging is from 4:00 to 8:00, and its discharging is from 11:00 to 15:00.

The heating hubs of the two cases are shown in Figure 7(c) and (d), respectively. The thermal demands are mainly met by auxiliary boiler, and the insufficient parts are provided by CHP. It can be seen that during the energy storage period of LAES (that is, 4:00 to 8:00), the compressor supplies part of the thermal energy. In addition to the thermal load, the absorption chiller also accounts for most of the thermal power output. The cooling hubs of the two cases are shown in Figure 7(e) and (f), respectively. The cold energy demand is mainly provided by the electric chiller, and the insufficient parts are met by the absorption chiller. The cold energy input from the LAES evaporation and the energy output from the cold energy hub to the LAES evaporation are also illustrated in the Figure 7(e) and (f).

Figure 8 shows the energy dispatching schedules of risk-neutral results with and without considering DRP. The comparison between the base load and the load using DRP is shown in Figure 8(a). With implementing the DRP, the peak at 15:00 is decreased to 19.77 kW. It should be noted that the total load is still 412.83 MWh no matter how the load changes in each time period. Figure 8(b) and (c) show the purchased power from the grid and natural gas system, respectively. In Figure 8(b), it can be seen that the amount of power purchased from grid at each time period of the day has changed when implementing the DRP. And in Figure 8(c), the amount of natural gas purchased at each time period is exactly the same.

Also, the stored energy of LAES is shown in Figure 8(d). The charging and discharging phases of LAES are shown in Figure 8(e). It can be seen that the charging and discharging time and

amount of the LAES system are exactly the same. This means that the DRP does not affect the scheduling of LAES system. From these five aspects, the strategy of purchasing power from the grid changed is the main reason for cost reduction after using DRP.

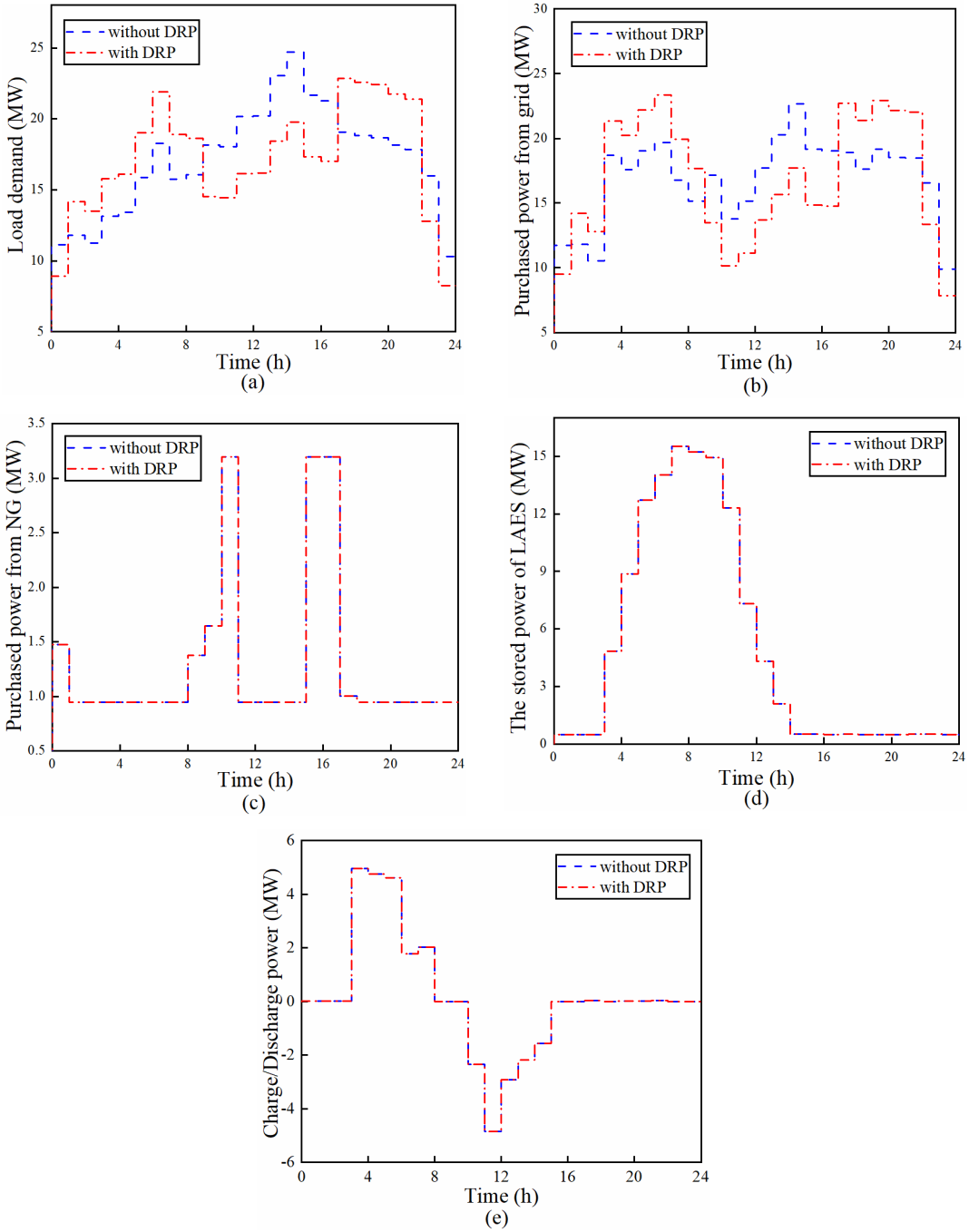

Figure 8. Energy dispatching strategies of risk-neutral results considering DRP in five aspects; (a) load profile, (b) the purchased power from grid, (c) the purchased power from natural gas system, (d) the stored power of LAES, (e) the charge/discharge power of LAES

In this study, to demonstrate the effectiveness of the proposed IGDT method in LAES-MES, stochastic programming [51] was carried out. Table 1 shows the economic cost of these two scheduling methods. As shown in Table 1, the IGDT method has a lower economic cost than

the stochastic programming scheduling method, in the case of without DRP and with DRP. Moreover, under the demand response, the economic cost has been reduced to a certain extent, which are 6.82% and 2.53% respectively. It should be noted that when applied to IGDT, the risk-neutral results mean that $\hat{\alpha}("\$"39390) = 0$ and $\hat{\beta}("\$"39390) = 0$ without implementing DRP. And, $\hat{\alpha}("\$"36702) = 0$ and $\hat{\beta}("\$"36702) = 0$ with implementing DRP.

Table 1. IGDT and Stochastic economic cost comparison

	IGDT		Stochastic	
	without DRP	with DRP	without DRP	with DRP
The expected economic cost ($)	39,390	36,702	39,462	38,462
The decreased economic cost by DRP ($)		2,688		1,000
The decreased economic cost by DRP (%)		6.82		2.53

The detailed scheduling strategies of IGDT and Stochastic programming methods are shown in Figure 9. The results of the two methods of purchasing power from the grid are illustrated in Figure 9(a) and (b). When the IGDT method is applied for dispatch, the total energy purchased from the grid is 405.68 MWh, which is 6.37 MWh more than 399.31 MWh in the stochastic programming. According to Figure 9(c) and (d), the decision to purchase natural gas for the two scheduling methods is basically the same, except the IGDT method is 1.07 MW higher at 11:00.

The liquid air energy storage status of the two scheduling methods is shown in Figure 9(e) and (f). In the IGDT method, the energy storage of the LAES system exceeds 15 MW, while in the stochastic programming method, the LAES system basically does not operate. It can be seen that the IGDT method can obtain lower cost through self-dispatching.

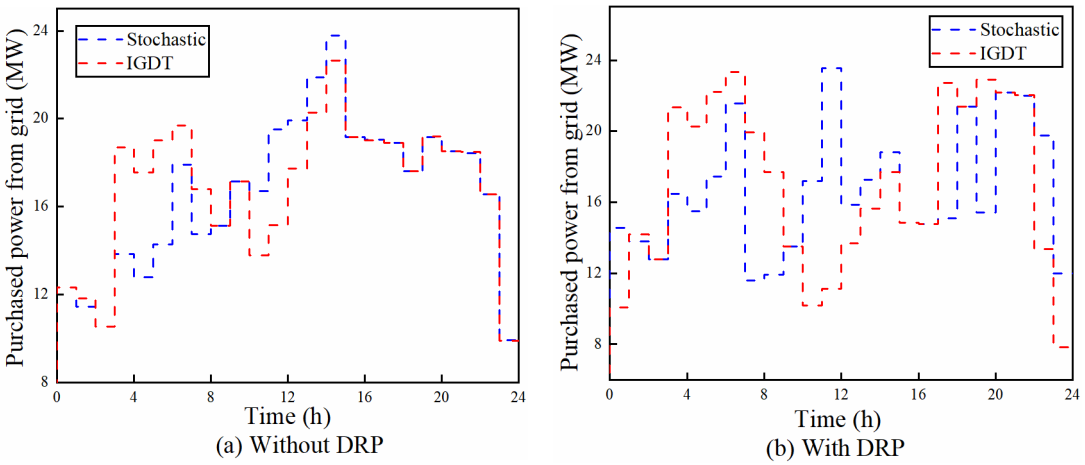

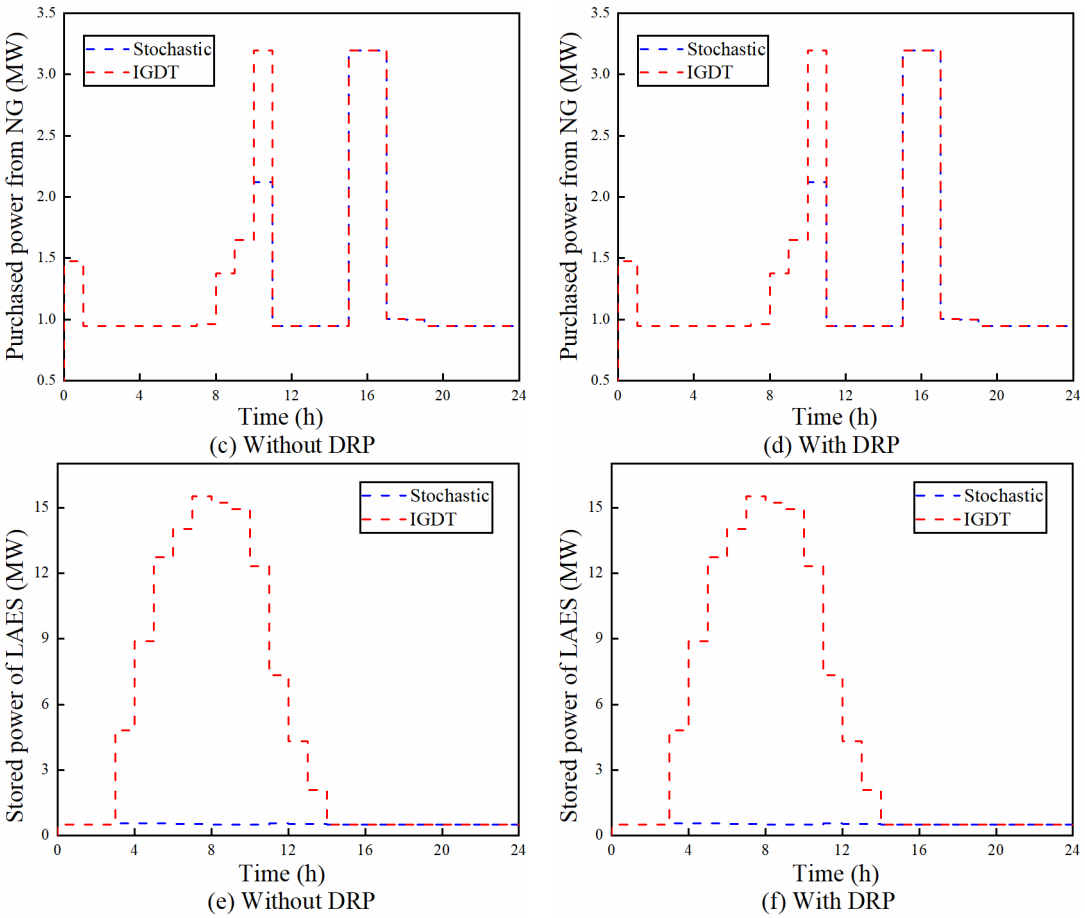

Figure 9. (a) Purchased power from grid without DRP, (b)Purchased power from grid with DRP, (c) Purchased power from NG without DRP, (d) Purchased power from NG with DRP, (e) Stored power of LAES without DRP, (f) Stored power of LAES with DRP.

5.3. Risk-based results

The robustness and opportunity function mentioned in Section 4 were applied to study the risk-averse strategy and risk-taker strategy. By solving these, the risk-based results of the two strategies are shown in Figure 10.

Opportunity function was used to develop a risk-taker strategy for decision-makers, who starve for a smaller cost. The results of opportunity function were obtained through solving $\hat{\beta}(R^t)$ which is detailed in Eq. (19), including scenarios considering without and with complementing DRP. As the opportunity cost changes, the changing trend of $\hat{\beta}(R^t)$ is depicted in Figure 10(a). As expected, $\hat{\beta}(R^t)$ increases as the opportunity cost R^t decreases whether or not DRP is implemented. In this study, the cost step was set as 800$.

Also, robustness function was used to develop a risk-averse strategy for operators, who are eager to acquire a stable cost. The results of robustness function were obtained by solving $\hat{\alpha}(R^a)$ which is detailed in Eq. (25), including scenarios considering with and without complementing DRP. As the robustness cost changes, the changing trend of $\hat{\alpha}(R^a)$ is depicted in Figure 10(b). As expected, $\hat{\alpha}(R^a)$ increases as the robustness cost R^a increases whether or not DRP is implemented. Also, it should be stated that the cost step was set as 800$ in this study.

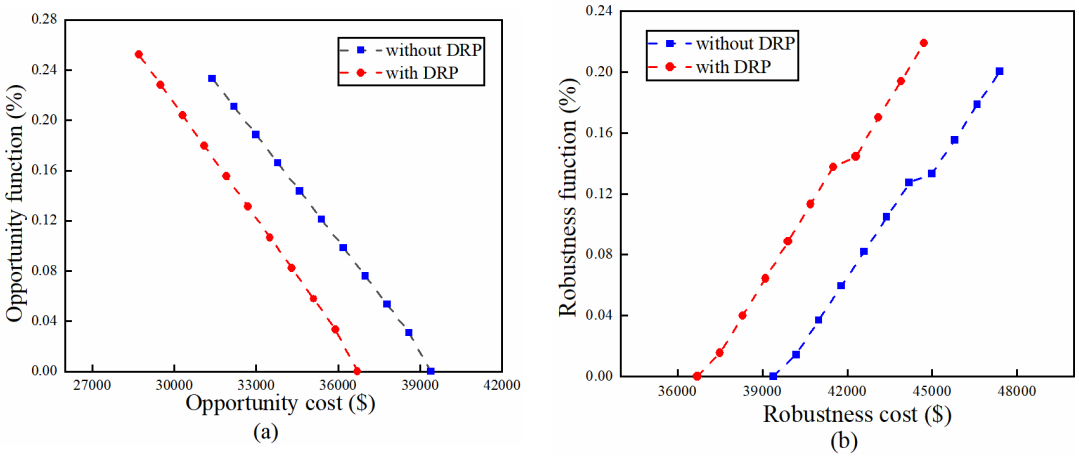

Figure 10. Risk-based results of LAES-MES based on IGDT; (a) Opportunity function, (b) Robustness function.

To deal with the uncertain electricity prices, different energy dispatching schedules were proposed to meet various cost demands, which are shown in Figure 11.

Figure 11 shows the purchased electricity from the grid in the risk-taker strategy and risk-averse strategy for a day, respectively. As the opportunity cost decreases, the total purchased power from the grid is shown an increasing trend in the risk-taker strategy (Figure 11(a)). Similar phenomenon was observed in the risk-averse strategy, that is, the power purchased from the grid is opposite to the increasing trend of opportunity cost. As the robustness cost increases, the total purchased power from the grid is on a downward trend (Figure 11(b)). The amount of power purchased from the grid shows a relatively large change among the change in some cost points. For example, with considering DRP, the system purchased 396.76 MWh from the grid a day when the opportunity cost is $33,502. This amount increases to 398.48 MWh when the opportunity cost decreases to $32,702.

Also, Figure 11(c) and (d) show the purchased power from natural gas system in the risk-taker and the risk-averse strategy for a day, respectively. In contrast to the increase in power purchased from grid as the opportunity cost decreases, the total purchased power from natural gas system reduces following the opportunity cost reduction (Figure 11(c)). In the risk-averse strategy, the total purchased power from natural gas system increases following the increase in the robustness cost (Figure 11(d)). The amount of power purchased from the natural gas system also shows a relatively large change among the change in some cost points. For example, without considering DRP, the system purchased 34.54 MWh from the natural gas system a day when the robustness cost is $44,190. This amount increases to 46.32 MWh when the opportunity cost increases to $44,990.

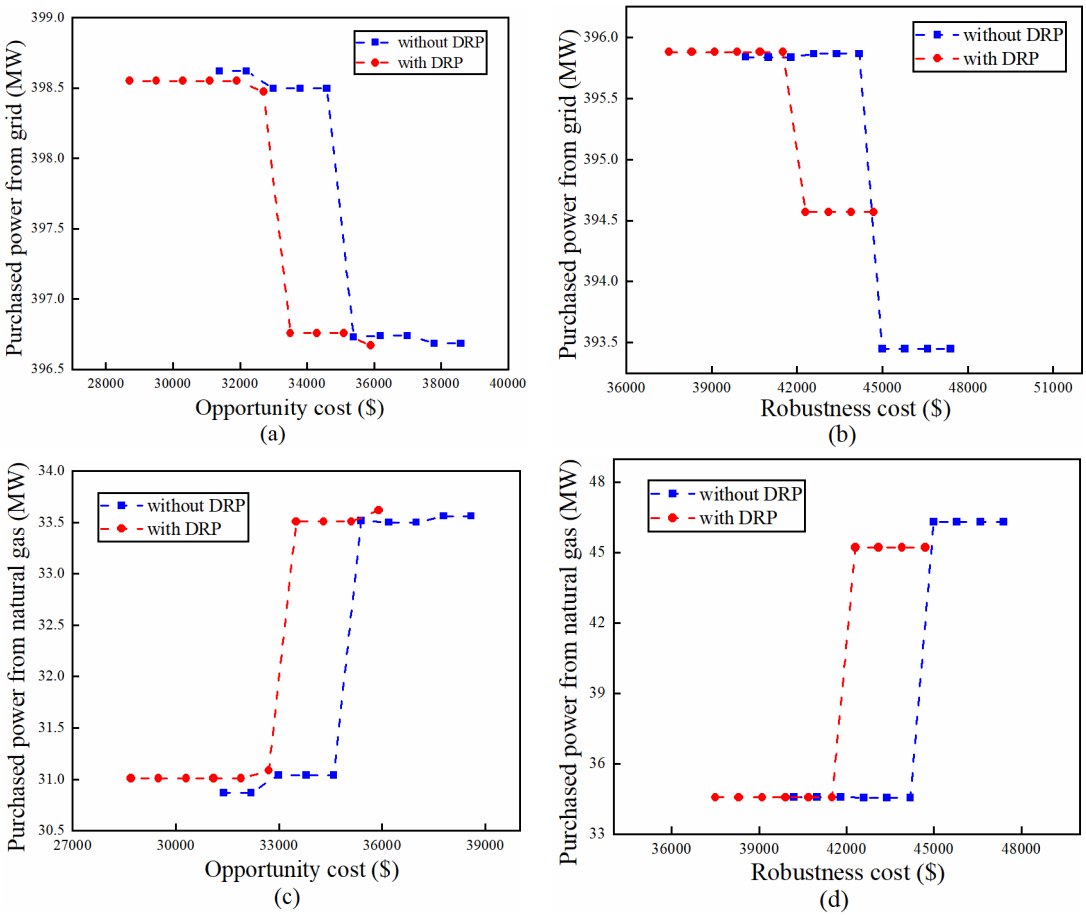

Figure 11. Power dispatching strategies; (a) Purchased power from grid of risk-averse strategy, (b) Purchased power from grid of risk-taker strategy, (c) Purchased power from natural gas system of risk-averse strategy, (d) Purchased power from natural gas system of risk-taker strategy.

Here, the power dispatching schedules of the hybrid energy system about four scenarios are showed in detail.

Scenario 1 (S1): Opportunity cost is $31,390 without complementing DRP

Scenario 2 (S2): Opportunity cost is $28,702 with complementing DRP

Scenario 3 (S3): Robustness cost is $47,390 without complementing DRP

Scenario 4 (S4): Robustness cost is $44,702 with complementing DRP

Figure 12(a) and (b) show the purchased power from the grid and natural gas system of four cases for a day, respectively. In Figure 12(a), the total purchased power from the grid in S1 is 398.62 MWh, 0.96% more than S3, in which the total purchased power from the grid is 394.78 MWh. And the total purchased power from the grid in S2 is 398.55 MWh, 0.93% more than S4, in which the total purchased power from the grid is 394.85 MWh. According to Figure 12(a), the total purchased power from the grid in risk-taker strategies are more than that in risk-averse strategies due to the lower electricity prices. Figure 12(b) shows that more power from the natural gas system is purchased in the strategies S3 and S4, compared with that of S1 and S2. During these risk-averse strategies, allowable uncertain electricity prices are higher than that of risk-taker strategies. This means it is more economical to purchase more natural gas for dispatch

than power obtained from the grid at high electricity prices.

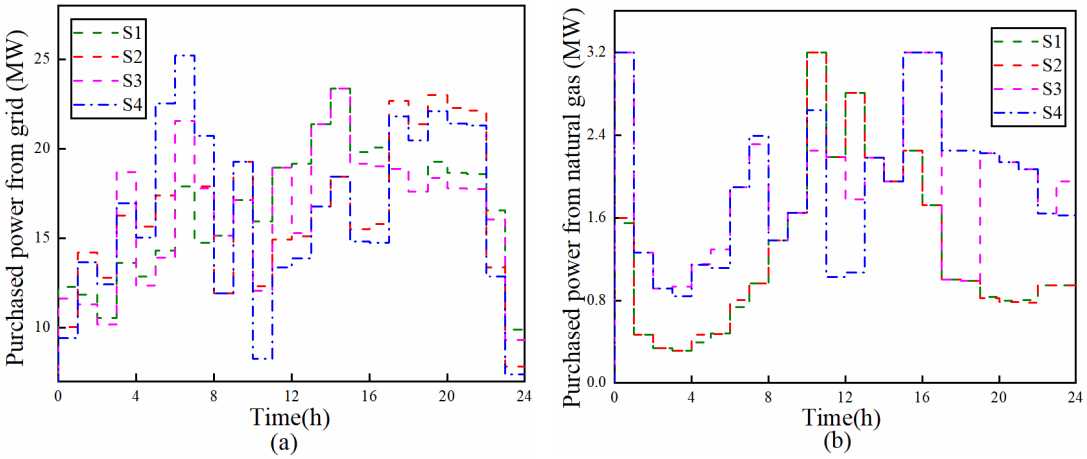

Figure 12. Purchasing strategies of four cases; (a) Purchased power from grid, (b) Purchased power from natural gas system.

6. Conclusion

In this paper, an energy scheduling strategy about an integrated system of liquid air energy system and multi-energy system was proposed to optimize system operation, reduce system economic cost and improve the ability to resist risks. The cold and heat circulation system of liquid air energy system interacted with the converter components of the combined cooling, heating and power system, to realize the integrated use of cold and thermal energy. In addition, three strategies, including risk-neutral, risk-taker and risk-averse strategy, were proposed to meet the need of decision-makers to consider uncertain electricity prices based on the IGDT method. The effectiveness of the IGDT method is obtained through comparative experiments. Moreover, demand response program (DRP) was applied to reduce peak-to-valley difference, reduce energy purchasing costs and decrease economic cost of the system finally. From two base cases (i.e. risk-neutral strategy), the predicted total cost with implementing DRP goes down from \$39,390 to \$36,702, which is 6.82% lower than the case without implementing DRP. Under the premise of meeting the expected cost, two different strategies (i.e. risk-taker and risk-averse strategy) were proposed to deal with the uncertainty of electricity prices. In the risk-taker strategy, the maximum allowable drop of electricity prices increases as the opportunity cost decreases. In the risk-averse strategy, the maximum allowable amplification of electricity prices increases as the opportunity cost increases. Through a detailed comparison of the purchase schedules in the four scenarios, the results show that replacing the grid with a natural gas system to provide power when the prices of electricity are high, was the energy purchasing solution to reduce the total economic cost.

Acknowledgements

This work was supported by National Natural Science Foundation of China (61973322).

Declarations of interest: none

Nomenclature

Abbreviations

LAES	Liquid Air Energy Storage
TES	Thermal Energy Storage
CES	Cold Energy Storage
NOCT	Nominal Operating Cell Temperature

Variables

$Cost_g(t)$	cost of natural gas at each time period t	cent
$Cost_e(t)$	cost of electricity at each time period t	cent
$Cost_{es}(t)$	cost of electricity storage at each time period t	cent
$Cost_{cs}(t)$	cost of thermal energy storage at each time period t	cent
$Cost_{cs}(t)$	cost of cold energy storage at each time period t	cent
$E_{Load}(t)$	final electricity load at each time period t	kW
$E_{PV}(t)$	power generated from PV at time period t	kW
$E_{WT}(t)$	power generated from wind power at time period t	kW
$E_{Grid}(t)$	power purchased from Grid at time period t	kW
$E_{CHP}(t)$	power generated from CHP at time period t	kW
$E_{Pump}(t)$	power generated from cryogenic pump at time period t	kW
$E_{EC}(t)$	power input to electric chiller at time period t	kW
$E_{load}^{sh}(t)$	shifted electricity load at time period t	kW
$E_{ch}(t), E_{ch-final}(t)$	primary charge and final charge power of LAES at time period t	kW
$E_{dis}(t), E_{dis-final}(t)$	primary discharge and final discharge power of LAES at time period t	kW
$H_{Load}(t)$	thermal load at each time period t	kW
$H_{CHP}(t)$	power generated from CHP at time period t	kW
$H_{A.B}(t)$	power generated from auxiliary boiler at time period t	kW
$H_{Comp}(t)$	power generated from compression at time period t	kW
$H_{Exp}(t)$	power input to expansion at time period t	kW
$H_{Ab.chiller}(t)$	power input to absorption chiller at time period t	kW
$H_{ch}(t), H_{ch-final}(t)$	primary charge and final charge power of TES at time period t	kW
$H_{dis}(t), H_{dis-final}(t)$	primary discharge and final discharge power of TES at time period t	kW
$C_{Load}(t)$	thermal load at each time period t	kW
$C_{Ab.chiller}(t)$	power generated from CHP at time period t	kW
$C_{EC}(t)$	power generated from electric chiller at time period t	kW
$C_{Evap}(t)$	power generated from evaporation at time period t	kW
$C_{Ref}(t)$	power input to refrigeration at time period t	kW
$C_{ch}(t), C_{ch-final}(t)$	primary charge and final charge power of CES at time period t	kW
$C_{dis}(t), C_{dis-final}(t)$	primary discharge and final discharge power of CES at time period t	kW
$x(t)$, $y(t)$	The binary variables representing charge and discharge state of ES at time period t	
$u(t)$, $v(t)$	The binary variables representing charge and discharge state of TES at time period t	
$m(t)$, $n(t)$	The binary variables representing charge and discharge state of CES at time period t	

$Eng^{LAES}(t)$	stored level of LAES at time period t	kW
$Eng^{TES}(t)$	power stored level at time period t	kW
$Eng^{CES}(t)$	power stored level at time period t	kW
$P_{CHP}^{g}(t)$	natural gas consumed by CHP at time period t	kW
$P_{A.B}^{g}(t)$	natural gas consumed by auxiliary boiler at time period t	kW
$G_T(t)$	solar irradiance on the PV array at time period t	W m^{-2}
$T_c(t)$	temperature of PV cell	℃
$T_a(t)$	ambient temperature	℃
$DR(t)$	the percentage of base load for participation in DRP at time period t	%
$inc(t)$	rate of increased load at time period t	%

Parameters

$Pr_A(t)$	natural gas price for heat generation	cent kWh^{-1}
$Pr_C(t)$	natural gas price for electricity generation	cent kWh^{-1}
$Pr_e(t)$	electricity price at each time period t	cent kWh^{-1}
$\xi_{oc}^{LAES}, \xi_{oc}^{C}, \xi_{oc}^{H}$	cost of electrical storage, cooling storage and heating storage	cent kWh^{-1}
ξ^{PV}, ξ^{WT}	cost of photovoltaic and wind power	cent kWh^{-1}
$\xi^{A.B}, \xi^{Ab.chiller}, \xi^{EC}, \xi^{CHP}$	cost of CCHP	cent kWh^{-1}
$E_{load}^{b}(t)$	base electricity load at time period t	kW
$E_{CHP}^{\max}$	maximum power output from CHP	kW
$E_{EC}^{\max}$	maximum power output from electric chiller	kW
$C_{Ab.chiller}^{\max}$	maximum cold energy output from absorption chiller	kW
$E_{ch}^{\max}, E_{dis}^{\max}$	maximum power flow of charge and discharge of LAES	kW
$H_{ch}^{\max}, H_{dis}^{\max}$	maximum power flow of charge and discharge of TES	kW
$C_{ch}^{\max}, C_{dis}^{\max}$	maximum power flow of charge and discharge of CES	kW
$SOC_{LAES}^{\max}, SOC_{LAES}^{\min}$	maximum and minimum energy stored level of LAES	kW
$SOC_{TES}^{\max}, SOC_{TES}^{\min}$	maximum and minimum energy stored level of TES	kW
$SOC_{CES}^{\max}, SOC_{CES}^{\min}$	maximum and minimum energy stored level of CES	kW
GLC	gas line capacity	kW
$COP^{Ab.chiller}$	coefficient of absorption chiller performance	-
ξ_{oc}	cost ratio	-
η_{Pump}	operation efficiency of the cryogenic pump	-
η_{hp}	thermal energy production efficiency during compression	-
η_{hn}	proportion of thermal energy needed during expansion	-
η_{cp}	cold energy production efficiency during evaporation	-
η_{cn}	proportion of cold energy needed during refrigeration	-
η_{ch}	charge efficiency of LAES	-
η_{dis}	discharge efficiency of LAES	-
$\eta_{A.B}$	operation efficiency of auxiliary boiler	-
η_{CHP}^{e}	electricity production efficiency of CHP	-
η_{CHP}^{H}	thermal energy production efficiency of CHP	-
$\eta_{Pr_{ch}^{H}}^{H}, \eta_{Pr_{dis}^{H}}^{H}$	charge and discharge efficiencies in PTCUH	-
$\eta_{Pr_{ch}^{C}}^{C}, \eta_{Pr_{dis}^{C}}^{C}$	charge and discharge efficiencies in PTCUC	-

τ	transmittance of PV cover	-
α	solar absorptance of PV array	-
α_p	temperature coefficient	-
Y_{PV}	rated capacity of PV array	kW
f_{PV}	derating factor	-
η_c	conversion efficiency of PV array	-
η_{inv}	inverter efficiency	-
ω_{rated}^{w}	rated speed of WT	m s^{-1}
ω_{out}^{cut}	cut out speed states of WT	m s^{-1}
ω_{in}^{cut}	cut in speed states of WT	m s^{-1}
Functions		
Γ	the economic cost function of LAES-MES	$
$\widehat{\alpha}(R^a)$	robustness function of IGDT	%
$\hat{\beta}(R^t)$	opportunity function of IGDT	%

Appendix A.

Table A.1. Constrains on subsystems

Subsystems	Description	Constrains	
Hub constraints	The balance of electrical power, thermal energy and cold energy sections.	$E_{PV}(t)+E_{WT}(t)+E_{Grid}(t)+E_{CHP}(t)+E_{dis-final}(t)=E_{Load}(t)+E_{ch}(t)+E_{EC}(t)$	(A.1)
		$H_{CHP}(t)+H_{A.B}(t)+H_{Comp}(t)+H_{dis-final}(t)=H_{ch}(t)+H_{Ab.chiller}(t)+H_{Exp}(t)+H_{load}(t)$	(A.2)
		$C_{Ab.chiller}(t)+C_{EC}(t)+C_{Evap}(t)+C_{dis-final}(t)=C_{ch}(t)+C_{Ref}(t)+C_{load}(t)$	(A.3)
LAES constraints	Charging and discharging ranges of the proposed LAES-MES are provided by Constraints. (A.4) and (A.5), respectively. Constraint. (A.6) is presented in order to prevent charge and discharge at the same time of the cryogenic tank in the LAES. The final charging energy to the tank and the final discharging energy from the expansion are detailed in Constraints. (A.7) and (A.8), respectively. During the discharging phase, liquid air needs to be pumped out by the cryogenic pump, which is shown in Constraint. (A.9). Also, the transmission of thermal and cold energy during the charging and discharging phases of LAES are depicted in Constraints. (A.10) - (A.13). During the charging phase, Kapitza cycle act as a recuperative process [52]. In this study, the aim is to recover the waste heat generated during the compression and supply waste heat to the expansion of LAES system, the absorption chiller and the thermal load. The thermal energy generated during the compression is shown in Constraint. (A.10). Constraint. (A.11) shows thermal energy needed during the expansion. During the	$0 \le E_{ch}(t) \le E_{ch}^{\max} \times x(t)$	(A.4)
		$0 \le E_{dis}(t) \le E_{dis}^{\max} \times y(t)$	(A.5)
		$x(t)+y(t) \le 1$	(A.6)
		$E_{ch-final}(t)=\eta_{ch} \times E_{ch}(t)$	(A.7)
		$E_{dis-final}(t)=\eta_{dis} \times E_{Pump}(t)$	(A.8)
		$E_{Pump}(\mathrm{t})=\eta_{Pump} \times E_{dis}(t)$	(A.9)
		$H_{Comp}=\eta_{hp} \times E_{ch}(t)$	(A.10)
		$H_{Exp}=\eta_{hn} \times E_{dis-final}(t)$	(A.11)
		$C_{Evap}=\eta_{cp} \times E_{dis}(t)$	(A.12)
		$C_{Ref}=\eta_{cn} \times E_{ch-final}(t)$	(A.13)
		$Eng^{LAES}(t)=Eng^{LAES}(t-1)+E_{ch-final}(t)-E_{dis}(t)$	(A.14)
		$SOC_{LAES}^{\min} \le Eng^{LAES}(\mathrm{t}) \le SOC_{LAES}^{\max}$	(A.15)
		$Eng_{loss}^{LAES}(t)=\gamma_{loss}^{E} Eng^{LAES}(t)$	(A.16)

	discharging phase, a working fluid R218 (C_3F_8) recovers the cold during the evaporation and provides cold energy to the LAES-MES [53]. Constraint. (A.12) expresses the cold energy generated from evaporation. The cold energy needed during the process of refrigerating air to liquid air is depicted in Constraint. (A.13). Constraint. (A.14) corresponds to the energy balance in the LAES at each time period t and the upper and lower limits of the stored energy are given by Constraint. (A.15). The energy loss of LAES system is shown by Constraint. (A.16).		
TES constraints	The heat the compressor, the expansion, CHP and AB produced can be stored in the thermal energy storage (TES) system, in order to use it conveniently. Like the LAES, the constraints of this system are stated in Constraints. (A.17) - (A.24). Constraint. (A.19) is presented in order to prevent charge and discharge at the same time in the TES. The final charging thermal energy to the TES system and the final discharging energy to the heating hub are detailed in Constraints. (A.20) and (A.21), respectively.	$0 \le H_{ch}(t) \le H_{ch}^{\max} \times u(t)$	(A.17)
		$0 \le H_{dis}(t) \le H_{dis}^{\max} \times v(t)$	(A.18)
		$u(t) + v(t) \le 1$	(A.19)
		$H_{ch-final}(\mathrm{t}) = \eta_{Pr_{ch}^{H}}^{H} \times H_{ch}(\mathrm{t})$	(A.20)
		$H_{dis-final}(t) = \eta_{Pr_{dis}^{H}}^{H} \times H_{dis}(t)$	(A.21)
		$Eng^{TES}(t) = Eng^{TES}(t-1) + H_{ch-final}(t) - H_{dis}(t)$	(A.22)
		$SOC_{TES}^{\min} \le Eng^{TES}(\mathrm{t}) \le SOC_{TES}^{\max}$	(A.23)
		$Eng_{loss}^{TES}(t) = \gamma_{loss}^{T} Eng^{TES}(t)$	(A.24)
CES constraints	The cold energy the evaporation, absorption chiller (Ab.chiller), and electric chiller (EC) produced can be stored in the cold energy storage (CES) system, in order to use it conveniently. Like the TES, the constraints of this system are stated in Constraints. (A.25) - (A.32).	$0 \le C_{ch}(\mathrm{t}) \le C_{ch}^{\max} \times m(t)$	(A.25)
		$0 \le C_{dis}(t) \le \mathrm{C}_{dis}^{\max} \times n(t)$	(A.26)
		$m(t) + n(t) \le 1$	(A.27)
		$C_{ch-final}(t) = \eta_{Pr_{ch}^{C}}^{\mathrm{C}} \times C_{ch}(t)$	(A.28)

	Constraint. (A.27) is presented to prevent charge and discharge at the same time in the CES. The final charging cold energy to the CES system and the final discharging energy to the cold hub are detailed in Constraints. (A.28) and (A.29), respectively.	$C_{dis-final}(t) = \eta^{C}_{Pr^{C}_{dis}} \times C_{dis}(t)$	(A.29)
		$Eng^{CES}(t)=Eng^{CES}(t-1) + C_{ch-final}(t) - C_{dis}(t)$	(A.30)
		$SOC^{\min}_{CES} \le Eng^{CES}(t) \le SOC^{\max}_{CES}$	(A.31)
		$Eng^{CES}_{loss}(t)=\gamma^{C}_{loss} Eng^{CES}(t)$	(A.32)
CCHP constraints	Constraint. (A.33) calculate the amount of fuel used by auxiliary boiler (A.B) with respect to its heat generation at each time period t. The power generated by CHP is an alternative choice except purchasing power from the grid in case of insufficient supply demand. The gas consumption value of CHP and the heat generated by CHP are determined by Constraints. (A.34) and (A.35), respectively. The allowable generating range of CHP is depicted in Constraint. (A.36). The consumption constraint of gas auxiliary boiler and CHP produce is shown by Constraint. (A.37). Constraints. (A.38) and (A.39) indicate the constraints of cold dispatching paths of Ab.chiller. The conversion of thermal to cooling energy occurring in the EC is depicted in Constraint. (A.40). Constraint. (A.41) determines the constraint of power to the EC.	$H_{A.B}(t) = \eta_{A.B} \times P^{g}_{A.B}(t)$	(A.33)
		$P^{g}_{CHP}(t)=\dfrac{E_{CHP}(t)}{\eta^{e}_{CHP}}$	(A.34)
		$H_{CHP}(t)=\eta^{H}_{CHP} \times P^{g}_{CHP}(t)$	(A.35)
		$0 \le E_{CHP}(t) \le E^{\max}_{CHP}$	(A.36)
		$P^{g}_{A.B}(t) + P^{g}_{CHP}(t) \le GLC$	(A.37)
		$C_{Ab.chiller}(t) = H_{Ab.chiller}(t) \times COP^{Ab.chiller}$	(A.38)
		$0 \le C_{Ab.chiller}(t) \le C^{\max}_{Ab.chiller}$	(A.39)
		$C_{EC}(t)=\eta_{EC} \times E_{EC}(t)$	(A.40)
		$0 \le E_{EC}(t) \le E^{\max}_{EC}$	(A.41)
Generation constraints of PV	The power output of the PV array in HOMER [54] was calculated using Constraints. (A.42) and (A.43).	$E_{P}(t) = Y_{PV} \times f_{PV} \times (\dfrac{G_{T}(t)}{G_{T,STC}}) \times [1+\alpha_{p} \times (T_{c} - T_{c,STC})]$	(A.42)

and Wind power	Constraint. (A.43) calculate the PV cell temperature using the energy balance for the PV array. The final power generation of PV panels is calculated using an efficiency of η_{inv} is shown by Constraint. (A.44). The power output of the wind power is calculated using Constraint. (A.45) [48].	$T_c(t) = T_a(t) + G_T(t) \times (\frac{T_{c,NOCT} - T_{\alpha,NOCT}}{\mathrm{G}_{T,NOCT}}) \times (1 - \frac{\eta_c}{\tau\alpha})$	(A.43)
		$E_{PV}(t) = \eta_{inv} \times E_P(t)$	(A.44)
		$E_{WT}(\omega(t)) = \begin{cases} E_{out}^w, & \omega_{rated}^w \le \omega(t) \le \omega_{out}^{cut} \\ \frac{\omega(t) - \omega_{in}^{cut}}{\omega_{rated}^w - \omega_{in}^{cut}}(E_{out}^w), & \omega_{in}^{cut} \le \omega(t) \le \omega_{rated}^w \\ 0, & \omega(t) \le \omega_{in}^{cut} \text{ or } \omega(t) \ge \omega_{out}^{cut} \end{cases}$	(A.45)

Appendix B.

Table B.1. System specifications

Parameters	Value	Units
LAES system [10, 55]		
$E_{ch}^{\max}$	5	MW
$E_{dis}^{\max}$	5	MW
η_{ch}	85	%
η_{dis}	90	%
η_{Pump}	80	%
η_{hp}	15	%
η_{cn}	25	%
η_{cp}	15	%
η_{hn}	25	%
$SOC_{LAES}^{\min}$	0.5	MW
$SOC_{LAES}^{\max}$	20	MW
γ_{LAES}^{loss}	0.02	-
TES system [56]		
$H_{ch}^{\max}$	5	MW
$H_{dis}^{\max}$	5	MW
$\eta_{Pr_{ch}^{H}}^{H}$	95	%
$\eta_{Pr_{dis}^{H}}^{H}$	95	%
$SOC_{TES}^{\min}$	0.2	MW
$SOC_{TES}^{\max}$	2	MW
γ_{TES}^{loss}	0.02	-
CES system [56]		
$C_{ch}^{\max}$	5	MW
$C_{dis}^{\max}$	5	MW
$\eta_{Pr_{ch}^{C}}^{C}$	92	%
$\eta_{Pr_{dis}^{C}}^{C}$	92	%
$SOC_{CES}^{\min}$	0.2	MW
$SOC_{CES}^{\max}$	2	MW
γ_{CES}^{loss}	0.02	-
PV system [57]		
Y_{PV}	1500	kW
f_{PV}	80	%
α_p	-0.5	-
$T_{c,STC}$	25	℃
$T_{c,NOCT}$	47	℃
η_c	13	%
τ	14.8	kW $m^{-2}K^{-1}$
α	30	%
η_{inv}	90	%

Wind power system [58]

E_{out}^{w}	1500	kW
ω_{rated}^{w}	13	m s^{-1}
ω_{out}^{cut}	25	m s^{-1}
ω_{in}^{cut}	3	m s^{-1}

Other parameters

[56]

ξ_{oc}^{E}	2.5	cent kWh^{-1}
ξ_{oc}^{C}	2.5	cent kWh^{-1}
ξ_{oc}^{H}	2.5	cent kWh^{-1}
ξ^{PV}	0.007	cent kWh^{-1}
ξ^{WT}	0.005	cent kWh^{-1}
$\xi^{A.B}$	0.001	cent kWh^{-1}
$\xi^{Ab.chiller}$	0.001	cent kWh^{-1}
ξ^{EC}	0.001	cent kWh^{-1}
ξ^{CHP}	0.011	cent kWh^{-1}
$E_{CHP}^{\max}$	900	kW
$E_{EC}^{\max}$	800	kW
$H_{A.B}^{\max}$	900	kW
$C_{Ab.chiller}^{\max}$	1000	kW
$\eta_{A.B}$	95	%
η_{CHP}^{e}	40	%
η_{CHP}^{H}	35	%
η_{EC}	85	%
GLC	6400	kW
$COP^{Ab.chiller}$	75	%

References

[1] "Organization of the Petroleum Exporting Countries.". http://www.opec.org/; [accessed 13 December 2019].

[2] Mancarella P. MES (multi-energy systems): An overview of concepts and evaluation models. Energy 2014; 65: 1-17. https://doi.org/10.1016/j.energy.2013.10.041.

[3] Lisbona D, Snee T. A review of hazards associated with primary lithium and lithium-ion batteries. Process Saf Environ Prot 2011; 89(6): 434-442. https://doi.org/10.1016/j.psep.2011.06.022.

[4] Sabihuddin S, Kiprakis AE, Mueller M. A Numerical and Graphical Review of Energy Storage Technologies. Energies. 2015;8(1):172-216. https://doi.org/10.3390/en8010172.

[5] Rodrigues E M G, Godina R, Santos S F, Bizuayehu A W, Contreras J, Catalão J P S. Energy storage systems supporting increased penetration of renewables in islanded systems. Energy 2014; 75: 265-280. https://doi.org/10.1016/j.energy.2014.07.072.

[6] Rehman S, Al-Hadhrami L M, Alam M M. Pumped hydro energy storage system: A technological review. Renew Sustain Energy Rev 2015; 44: 586-598. https://doi.org/10.1016/j.rser.2014.12.040.

[7] Yao E, Wang H, Wang L, Xi G, Maréchal F. Multi-objective optimization and exergoeconomic analysis of a combined cooling, heating and power based compressed air energy storage system. Energy Convers Manage 2017; 138: 199-209. https://doi.org/10.1016/j.enconman.2017.01.071.

[8] Venkataramani G, Parankusam P, Ramalingam V, Wang J. A review on compressed air energy storage – A pathway for smart grid and polygeneration[J]. Renew Sustain Energy Rev 2016: 895-907. https://doi.org/10.1016/j.rser.2016.05.002.

[9] Evans A, Strezov V, Evans T J. Assessment of utility energy storage options for increased renewable energy penetration. Renew Sustain Energy Rev 2012; 16(6): 4141-4147. https://doi.org/10.1016/j.rser.2012.03.048.

[10] Morgan R, Nelmes S, Gibson E, Brett G. Liquid air energy storage – Analysis and first results from a pilot scale demonstration plant. Appl Energy 2015; 137: 845-853. https://doi.org/10.1016/j.apenergy.2014.07.109.

[11] http://www.highview-power.com/; [accessed 01 August 2016].

[12] Yang Y. Development of the worlds largest above ground full containment LNG storage tank. In: 23rd World gas conference2006: Amsterdam.

[13] Tafone A, Borri E, Comodi G, van den Broek M, Romagnoli A. Liquid Air Energy Storage performance enhancement by means of Organic Rankine Cycle and Absorption Chiller. Appl Energy 2018; 228: 1810-1821. https://doi.org/10.1016/j.apenergy.2018.06.133.

[14] Ameel B, T'Joen C, De Kerpel K, De Jaeger P, Huisseune H, Van Belleghem M, De Paepe M. Thermodynamic analysis of energy storage with a liquid air Rankine cycle. Appl Therm Eng 2013; 52(1): 130-140. https://doi.org/10.1016/j.applthermaleng.2012.11.037.

[15] Zhang T, Chen L, Zhang X, Mei S, Xue X, Zhou Y. Thermodynamic analysis of a novel hybrid liquid air energy storage system based on the utilization of L

NG cold energy. Energy 2018; 155: 641-650. https://doi.org/10.1016/j.energy.2018.05.041.

[16] Rehman A, Qyyum MA, Qadeer K, Zakir F, Ding YL, Lee M, Wang L. Integrated biomethane liquefaction using exergy from the discharging end of a liquid air energy storage system. Appl Energy. 2020; 260: 12. https://doi.org/10.1016/j.apenergy.2019.114260.

[17] Li Y, Cao H, Wang S, Jin Y, Li D, Wang X, Ding Y. Load shifting of nuclear power plants using cryogenic energy storage technology. Appl Energy 2014; 113: 1710-1716. https://doi.org/10.1016/j.apenergy.2013.08.077.

[18] Cao S, Hasan A, Sirén K. On-site energy matching indices for buildings with energy conversion, storage and hybrid grid connections. Energy Build 2013; 64: 423-438. https://doi.org/10.1016/j.enbuild.2013.05.030.

[19] Zhang S, Huang P, Sun Y. A multi-criterion renewable energy system design optimization for net zero energy buildings under uncertainties. Energy 2016; 94: 654-665. https://doi.org/10.1016/j.energy.2015.11.044.

[20] Wang B, Zhou M, Xin B, Zhao X, Watada J. Analysis of operation cost and wind curtailment using multi-objective unit commitment with battery energy storage. Energy 2019; 178: 101-114. https://doi.org/10.1016/j.energy.2019.04.108.

[21] Amiri S, Honarvar M, sadegheih A. Providing an integrated Model for Planning and Scheduling Energy Hubs and preventive maintenance. Energy 2018; 163: 1093-1114. https://doi.org/10.1016/j.energy.2018.08.046.

[22] Majidi M, Mohammadi-Ivatloo B, Soroudi A. Application of information gap decision theory in practical energy problems: A comprehensive review. Appl Energy 2019; 249: 157–65. https://doi.org/10.1016/j.apenergy.2019.04.144.

[23] Nojavan S, Majidi M, Najafi-Ghalelou A, Ghahramani M, Zare K. A cost-emission model for fuel cell/PV/battery hybrid energy system in the presence of demand response program: ε-constraint method and fuzzy satisfying approach. Energy Convers Manage 2017; 138: 383–92. https://doi.org/10.1016/j.enconman.2017.02.003.

[24] Liu Y, Li M, Lian H, Tang X, Liu C, Jiang C. Optimal dispatch of virtual power plant using interval and deterministic combined optimization. Int J Electr Power Energy Syst 2018; 102: 235–44. https://doi.org/10.1016/j.ijepes.2018.04.011.

[25] Zakariazadeh A, Jadid S, Siano P. Stochastic operational scheduling of smart distribution system considering wind generation and demand response programs. Int J Electr Power Energy Syst 2014; 63: 218–25. https://doi.org/10.1016/j.ijepes.2014.05.062.

[26] Jeong J, Lee B. A framework for estimating flexible resources according to future Korean renewables scenario: Robust optimization approach considering multiple uncertainties. Int J Electr Power Energy Syst 2020; 118: 105728. https://doi.org/10.1016/j.ijepes.2019.105728.

[27] Liang J, Tang W. Interval based transmission contingency-constrained unit commitment for integrated energy systems with high renewable penetration. Int J Electr Power Energy Syst 2020; 119: 105853. https://doi.org/10.1016/j.ijepes.2020.105853.

[28] Zeng B, Wei X, Sun B, Qiu F, Zhang J, Quan X. Assessing capacity credit of demand response in smart distribution grids with behavior-driven modeling framework. Int J Electr Power Energy Syst 2020; 118: 105745. https://doi.org/10.1016/j.ijepes.2019.105745.

[29] Nojavan S, Zare K. Optimal energy pricing for consumers by electricity retailer. Int J Electr Power Energy Syst 2018; 102: 401–12. https://doi.org/10.1016/j.ijepes.2018.05.013.

[30] Ghahramani M, Nazari-Heris M, Zare K, Mohammadi-Ivatloo B. Energy and reserve management of a smart distribution system by incorporating responsive-loads /battery/wind turbines considering uncertain parameters. Energy 2019; 183: 205–19. https://doi.org/10.1016/j.energy.2019.06.085.

[31] Vahid-Pakdel M J, Nojavan S, Mohammadi-ivatloo B, Zare K. Stochastic optimization of energy hub operation with consideration of thermal energy market and demand response. Energy Convers Manage 2017; 145: 117-128. https://doi.org/10.1016/j.enconman.2017.04.074.

[32] Moazeni S, Miragha A H, Defourny B. A Risk-Averse Stochastic Dynamic Programming Approach to Energy Hub Optimal Dispatch. IEEE Trans Power Syst 2019; 34(3): 2169-2178. https://doi.org/10.1109/TPWRS.2018.2882549.

[33] Park H, Baldick R. Stochastic Generation Capacity Expansion Planning Reducing Greenhouse Gas Emissions. IEEE Trans Power Syst 2015; 30(2): 1026-34. https://doi.org/10.1109/TPWRS.2014.2386872.

[34] Maghouli P, Hosseini SH, Buygi MO, Shahidehpour M. A Scenario-Based Multi-Objective Model for Multi-Stage Transmission Expansion Planning. IEEE Trans Power Syst 2011; 26(1): 470-8. https://doi.org/10.1109/TPWRS.2010.2048930.

[35] Moretti L, Martelli E, Manzolini G. An efficient robust optimization model for the unit commitment and dispatch of multi-energy systems and microgrids. Appl Energy 2020; 261: 24. https://doi.org/10.1016/j.apenergy.2019.113859.

[36] Aghamohamadi M, Mahmoudi A. From bidding strategy in smart grid toward integrated bidding strategy in smart multi-energy systems, an adaptive robust solution approach. Energy 2019; 183: 75-91. https://doi.org/10.1016/j.energy.2019.06.106.

[37] Info-Gap Decision Theory | Decisions Under Severe Uncertainty. https://info-gap.technion.ac.il/; [accessed 01 June 2019].

[38] Majidi M, Zare K. Integration of Smart Energy Hubs in Distribution Networks Under Uncertainties and Demand Response Concept. IEEE Trans Power Syst 2019; 34(1): 566-74. https://doi.org/10.1109/TPWRS.2018.2867648.

[39] Moghaddas-Tafreshi SM, Jafari M, Mohseni S, Kelly S. Optimal operation of an energy hub considering the uncertainty associated with the power consumption of plug-in hybrid electric vehicles using information gap decision theory. Int J Electr Power Energy Syst 2019; 112: 92-108. https://doi.org/10.1016/j.ijepes.2019.04.040.

[40] Dolatabadi A, Jadidbonab M, Mohammadi-ivatloo B. Short-Term Scheduling Strategy for Wind-Based Energy Hub: A Hybrid Stochastic/IGDT Approach. IEEE

Trans Sustain Energy 2019; 10(1): 438-48. https://doi.org/10.1109/TSTE.2017.2788086.

[41] Soroudi A, Rabiee A, Keane A. Information gap decision theory approach to deal with wind power uncertainty in unit commitment. Electr Power Syst Res 2017; 145: 137-48. https://doi.org/10.1016/j.epsr.2017.01.001.

[42] Nojavan S, Zare K, Ashpazi MA. A hybrid approach based on IGDT–MPSO method for optimal bidding strategy of price-taker generation station in day-ahead electricity market. Int J Electr Power Energy Syst 2015; 69: 335–43. https://doi.org/10.1016/j.ijepes.2015.01.006.

[43] Vatani B, Chowdhury B, Dehghan S, Amjady N. A critical review of robust self-scheduling for generation companies under electricity price uncertainty. Int J Electr Power Energy Syst 2018; 97: 428–39. https://doi.org/10.1016/j.ijepes.2017.10.035.

[44] Ghahramani M, Nojavan S, Zare K, Mohammadi-ivatloo B. Application of Load Shifting Programs in Next Day Operation of Distribution Networks. Operation of Distributed Energy Resources in Smart Distribution Networks, Elsevier; 2018, p. 161–77.

[45] Korkas C D, Baldi S, Michailidis I, Kosmatopoulos E B. Occupancy-based demand response and thermal comfort optimization in microgrids with renewable energy sources and energy storage. Appl Energy 2016; 163: 93-104. https://doi.org/10.1016/j.apenergy.2015.10.140

[46] Bagal H A, Soltanabad Y N, Dadjuo M, Wakil K, Ghadimi N. Risk-assessment of photovoltaic-wind-battery-grid based large industrial consumer using information gap decision theory. Sol Energy 2018; 169: 343-352. https://doi.org/10.1016/j.solener.2018.05.003.

[47] GAMS User's Guide. https://www.gams.com/latest/docs/UG_MAIN.html; [accessed 14 March 2019].

[48] Soroudi A, Aien M, Ehsan M. A Probabilistic Modeling of Photo Voltaic Modules and Wind Power Generation Impact on Distribution Networks. IEEE Syst J 2012; 6: 254–9. https://doi.org/10.1109/JSYST.2011.2162994.

[49] Aghbalou N, Charki A, Elazzouzi SR, Reklaoui K. A probabilistic assessment approach for wind turbine-site matching. Int J Electr Power Energy Syst 2018; 103: 497–510. https://doi.org/10.1016/j.ijepes.2018.06.018.

[50] Monteiro C, Ramirez-Rosado IJ, Fernandez-Jimenez LA, Ribeiro M. New probabilistic price forecasting models: Application to the Iberian electricity market. Int J Electr Power Energy Syst 2018; 103: 483–96. https://doi.org/10.1016/j.ijepes.2018.06.005.

[51] Powell WB, Meisel S. Tutorial on Stochastic Optimization in Energy—Part I: Modeling and Policies. IEEE Trans Power Syst 2016; 31: 1459–67. https://doi.org/10.1109/TPWRS.2015.2424974.

[52] Tafone A, Romagnoli A, Borri E, Comodi G. New parametric performance maps for a novel sizing and selection methodology of a Liquid Air Energy Storage system. Appl Energy 2019; 250: 1641–56. https://doi.org/10.1016/j.apenergy.2019.04.171.

[53] Hamdy S, Morosuk T, Tsatsaronis G. Cryogenics-based energy storage: Evaluation of cold exergy recovery cycles. Energy 2017; 138: 1069–80. https://doi.org/10.1016/j.energy.2017.07.118.

[54] HOMER help manual. http://www.homerenergy.com/pdf/HOMERHelpManual.pdf; [accessed 07 August 2019].

[55] Tafone A, Romagnoli A, Borri E, Comodi G. New parametric performance maps for a novel sizing and selection methodology of a Liquid Air Energy Storage system. Appl Energy 2019; 250: 1641–56. https://doi.org/10.1016/j.apenergy.2019.04.171.

[56] Rakipour D, Barati H. Probabilistic optimization in operation of energy hub with participation of renewable energy resources and demand response. Energy 2019; 173: 384–99. https://doi.org/10.1016/j.energy.2019.02.021.

[57] Soroudi A, Ehsan M. A possibilistic–probabilistic tool for evaluating the impact of stochastic renewable and controllable power generation on energy losses in distribution networks—A case study. Renew Sustain Energy Rev 2011; 15: 794–800. https://doi.org/10.1016/j.rser.2010.09.035.

[58] Baneshi M, Hadianfard F. Techno-economic feasibility of hybrid diesel/PV/wind/battery electricity generation systems for non-residential large electricity consumers under southern Iran climate conditions. Energy Convers Manage 2016; 127: 233–44. https://doi.org/10.1016/j.enconman.2016.09.008.